Highly Stretchable and Sensitive Strain Sensor based on Ag NWs-Elastomer Nanocomposite

*Morteza Amjadi[1,2,3], Aekachan Pichitpajongkit[1,2], Sangjun Lee[4], Seunghwa Ryu[1,2] and Inkyu Park[1,2,3]**

[1]Department of Mechanical Engineering, Korea Advanced Institute of Science and Technology (KAIST), Daejeon, South Korea

[2]KI for the NanoCentury, Korea Advanced Institute of Science and Technology (KAIST), Daejeon, South Korea

[3]Mobile Sensor and IT Convergence (MOSAIC) Center, Korea Advanced Institute of Science and Technology (KAIST), Daejeon, South Korea

[4]Department of Physics, Korea Advanced Institute of Science and Technology (KAIST), Daejeon, South Korea

[*]:inkyu@kaist.ac.kr

Mechanical properties of the AgNWs-PDMS nanocomposite: Elastic modulus of the PDMS medium was considered to be 1.64 MPa, and that of the AgNWs-PDMS nanocomposite layer was predicted by the Halpin–Tsai Equation.[1]

$$E = \frac{1 + 2.\frac{l_f}{d_f}\eta\varphi}{1 - \eta\varphi}.E_m$$

Here, l_f and d_f are the length (20 μm) and the diameter (150 nm) of AgNWs, $\varphi$is the volume fraction of AgNWs in the PDMS matrix, $E_m$is the shear modulus of the matrix and η is given by:

$$\eta = \frac{\frac{E_f}{E_m} - 1}{\frac{E_f}{E_m} + 2.\frac{l_f}{d_f}}$$

where $E_f$is the elastic modulus of bulk Ag. The calculated elastic modulus for the AgNWs-PDMS nanocomposite with a volume fraction of φ=5% is 6.32 MPa, which is 3.85 times larger than that of the PDMS matrix.

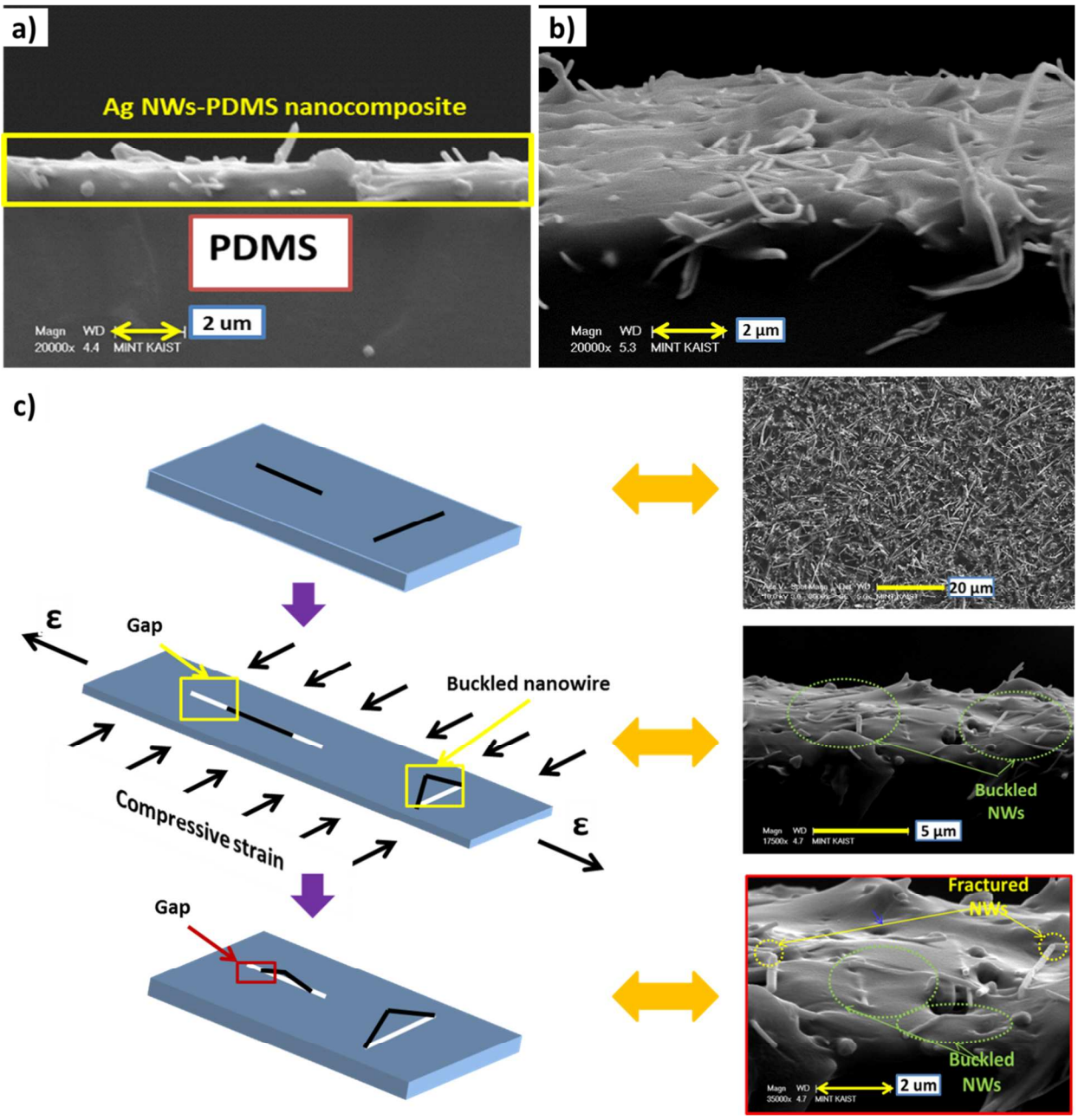

Figure S1. a) Highly cross-linked AgNW-PDMS nanocomposite on the PDMS layer. b) Permanent deformation and surface instability of the nanocomposite layer during stretching/releasing cycle. c) Buckling and fracture of AgNWs due to compressive strain in the transverse direction of stretch and friction force in the longitudinal direction of stretch.

Wire-PDMS composite model: Since the AgNWs-PDMS nanocomposite layer is covered by two layers of PDMS in the sandwich structured sample, it was impossible to take the SEM images on the surface of nanocomposite to monitor the morphology changes under strains. Toward these objectives, we prepared both simple and sandwich structured samples with a PDMS medium and copper (Cu) wires (average diameter=150 μm and length= 2 mm) as filler elements, as shown in Figure S2a. By using these samples, the movement of wires can be easily monitored with an optical microscope. Stretch/release cycles were then applied to samples while the morphological changes were recorded by an optical microspore. Figure S2b shows the random orientation of wires in the PDMS matrix. Figure S2c and d illustrate the morphological change of wires in the case of simple structured sample by the 40% of stretching. There are gaps between wires' tip and PDMS matrix due to much larger elongation of PDMS. Although the wires should slide back to their initial positions after releasing, the friction force between PDMS and wires prevent the position recovery.[2] As Figure S2e shows, the wires could not completely return to their original positions and gaps between the wire tips and PDMS remain after strain releasing. These gaps cause compressive stress to wires inducing out-of-plane buckling and fracture under cyclic loads. As Figure S2f depicts, many wires were ripped-off from PDMS after releasing the simple structured sample from strain, indicating out-of-plane buckling of wires. However, in the case of the sandwich structured sample, the structural integrity of the PDMS-wire composite is preserved. Figure panels S2g, h and j illustrate the morphology of wires in the case of the sandwich structured sample before, under and after stretch (□=40%) at the same spot, respectively. Under stretch, gap exists between two ends of wires and PDMS matrix; but, all wires completely followed back by their paths without any buckling and fracture, as indicated in Figure S2k.

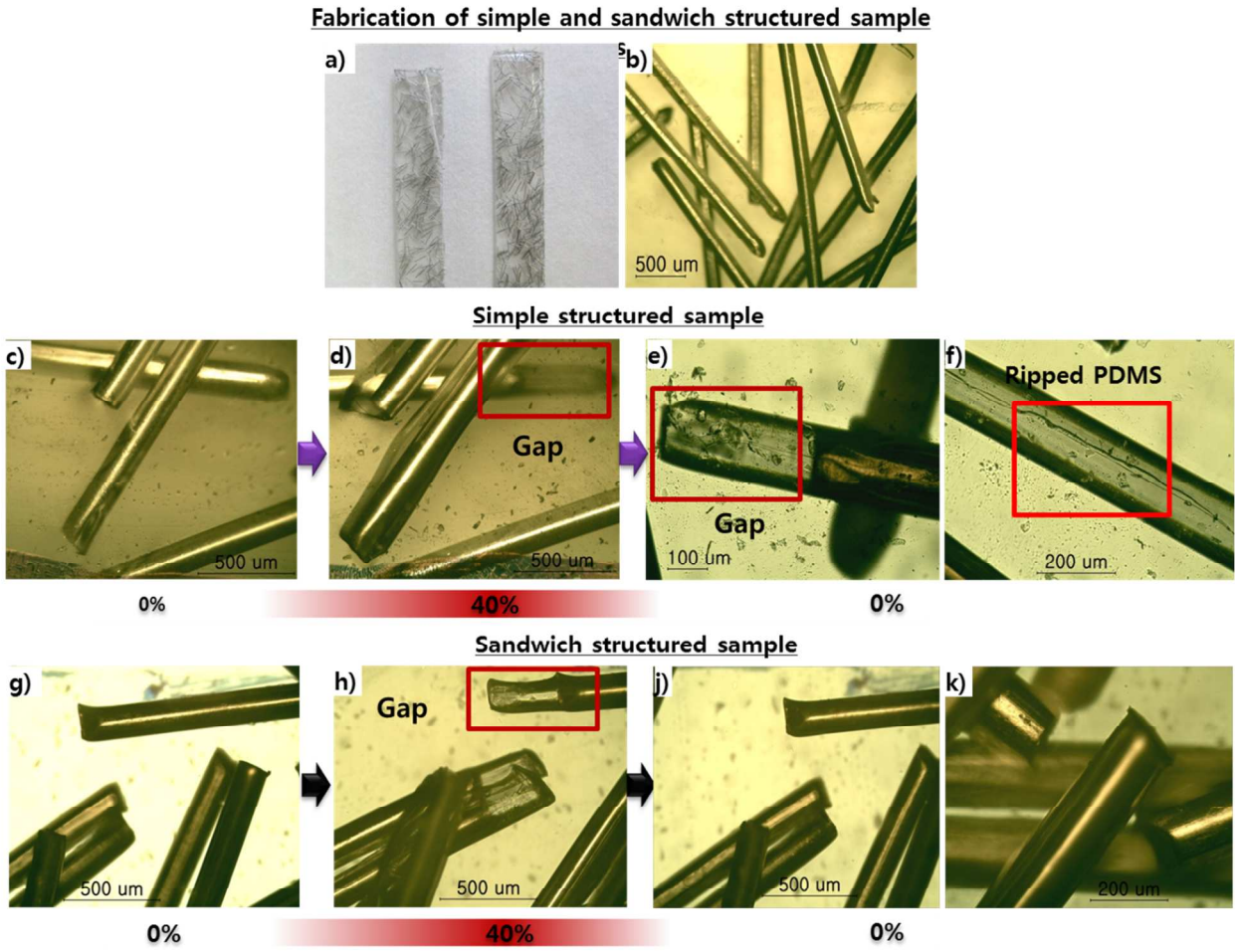

Figure S2. Wire-PDMS Composite Model: a) Fabricated simple and sandwich structured samples by using PDMS as medium and Cu wires as fillers. b) Random orientation of wires in the PDMS matrix. c and d) The morphology of wires' orientation in the case of simple structured sample before and under stretch at the same spot. e) Image of wire tip which partially slide back to its position after releasing. f) Ripped PDMS due to out-of-plane buckling of wire. g, h and j) The morphology of wires' orientation in the case of the sandwich structured sample before, under and after stretch at the same spot. k) Orientation of wires after releasing the sandwich structured sample; all wires slide back to their original locations.

Reliability test: We tested the performance of the strain sensors to the cyclic loading with both low and high strain levels. The response of a strain sensor to cyclic loading from 0 to 10% of strain for more than 225 cycles is illustrated in Figure S3a. As the figure depicts, the strain sensor responds to the cyclic loading with a good stability and reproducibility. Furthermore, we investigated performance of the strain sensors to higher strain levels (ε=10 % to 40 %) for more than 1000 cycles. The electrical current of strain sensor gradually was decreased by cyclic loading as shown in Figure S3b. The minimum resistance of the strain sensor after cyclic test was increased by ~ 6.25 %. We believe that this degradation is mainly caused by the fatigue of the PDMS substrate rather than the delamination of AgNWs from PDMS substrate since they are completely covered by PDMS layers in the top and bottom surfaces. In order to overcome this problem, we plan to replace the PDMS matrix with more stretchable polymer materials.

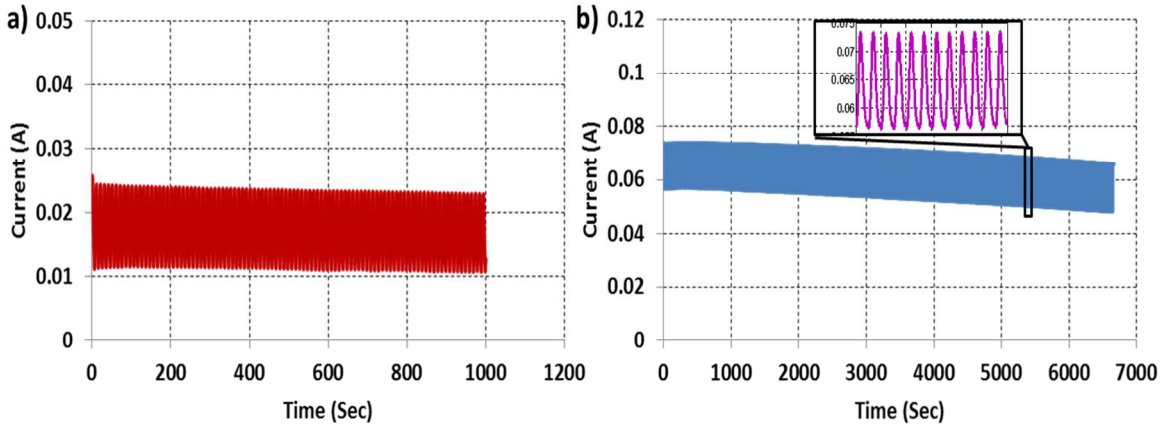

Figure S3. a) Cyclic test for low strain level (□=10%). b) Performance of a strain sensor to high level strains (from 10 to 40%).

Response time: To calculate response time of the strain sensor, we assumed that our strain sensor is a first order system. For a first order system:

$$\frac{\mathbf{C(S)}}{\mathbf{R(S)}} = \frac{\mathbf{1}}{\boldsymbol{\tau}\mathbf{S} + \mathbf{1}}$$

where τ is the time constant of the system, and C(S) and R(S) are the Laplace function for output and input, respectively.

For a ramp input:

$$\mathbf{R(S)} = \frac{\mathbf{k}}{\mathbf{S^2}}$$

Then:

$$\mathbf{C(S)} = \frac{\mathbf{k}}{\mathbf{S^2}(\boldsymbol{\tau}\mathbf{S} + \mathbf{1})}$$

By solving the equation:

$$\mathbf{C(t)} = \mathbf{k}(\mathbf{t} - \boldsymbol{\tau}\left(\mathbf{1} - \mathbf{e}^{\left(-\frac{\mathbf{t}}{\boldsymbol{\tau}}\right)}\right))$$

Ramp strain from 0% to 40% (with strain rate of 6.65 $mm.s^{-1}$) was applied to the strain sensor (see Figure S4a) while the response of the strain sensor was measured (see Figure S4b). Then, data was fitted by a first order system response as follow:

$$\mathbf{C(t)} = \mathbf{1.757}(\mathbf{t} - \mathbf{0.087}\left(\mathbf{1} - \mathbf{e}^{\left(-\frac{\mathbf{t}}{\mathbf{0.087}}\right)}\right))$$

The time constant τ for our strain sensors is ~ 0.087 s (87 ms). Therefore 90% time constant ($\tau_{90\%}$) is 200 ms. If we consider the unknown delay of the measurement system, the actual time constant for the sensor itself would be shorter than this.

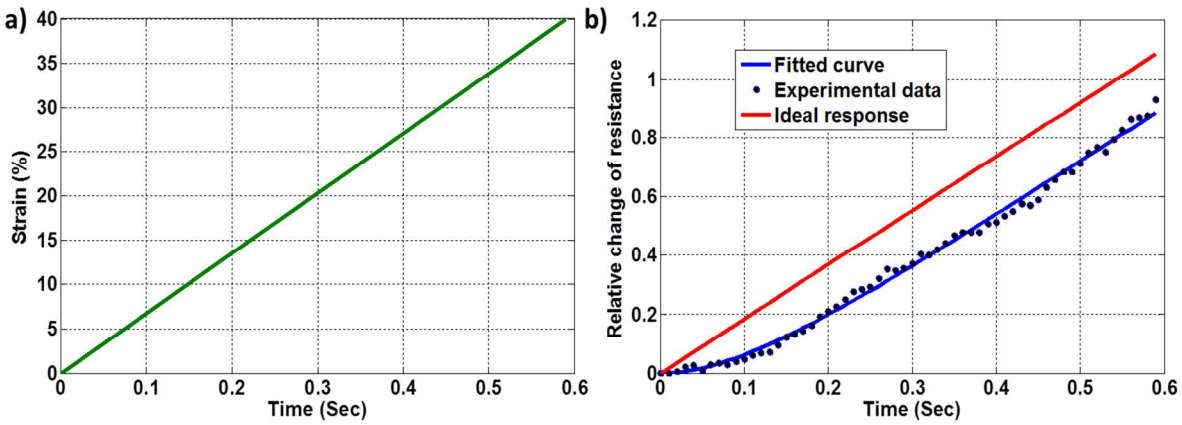

Figure S4. a) Ramp strain applied to the strain sensor. b) Experimental data from a strain sensor, best fitted curve and ideal response.

Nonlinearity and linearity: To investigate the nonlinearity in the high resistance strain sensors and linear response in the case of low resistance strain sensors, the number of current flowing NWs and topology changes of networks for both strain sensors are investigated. As shown in Figure S5a, the resistance of high resistance strain sensor increases nonlinearly by the applied strain. On the other hand, low resistance strain sensor shows a linear behavior. Furthermore, the number of current flowing NWs is linearly decreased by the applied strain for both high and low resistance strain sensors. However, the resistance of the low density AgNW network (~ 1500 NWs) is not dominated by the total number of current flowing NWs but by the topology of percolating NW clusters. As shown in Figure S5c, the AgNW network transforms from "homogeneous network" to "inhomogeneous network" with emerging bottleneck locations that critically limit the electrical current. This results in the nonlinear response of high resistance strain sensor to the applied strain as shown in Figure S5a. In contrast, highly linear behavior is observed in the strain sensor with low resistance due to dense AgNW network ((~ 2800 NWs) as shown in Figure S5a. In this case, no bottleneck locations for electrical current are observed in the AgNW network even for high strains up to 100% due to high number density of AgNWs as shown in Figure S5d. The AgNW network with high number density of NWs exhibits better connectivity between NWs. As a consequence, the emergence of bottleneck locations is less probable and the electrical resistance is linearly dependent on the number of current flowing NWs. Therefore, the strain sensor with low resistance shows highly linear response to the applied strain.

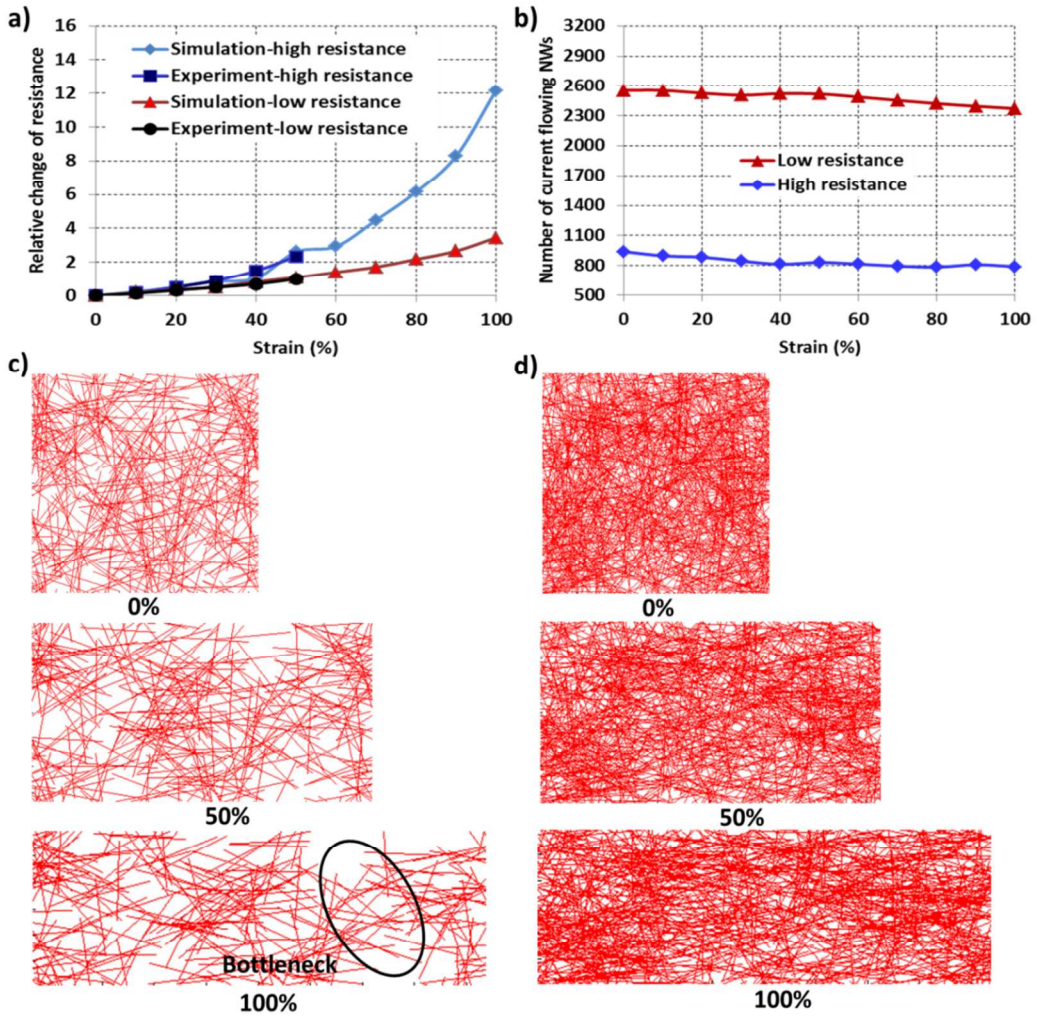

Figure S5. a) Piezoresistive response for high and low resistance strain sensors-both simulation and experiment. b) Decrease of the current flowing NWs for high and low resistance strain sensors. c) Top projected view of the AgNW network at different level of strain for a high resistance strain sensor with bottleneck location. d) Top projected view of the AgNW network at different level of strain for a low resistance strain sensor.

REFERENCE:

[1] Denver H.; Heiman, T.; Martin, E.; Gupta, A.; Borca-Tasciuc, D. A. Fabrication of Polydimethylsiloxane Composites with Nickel Nanoparticle and Nanowire Fillers and Study of Their Mechanical and Magnetic Properties. *J. Appl. Phys.* **2009**, 106, 064909.

[2] Xu, F.; Z., Yong. Highly Conductive and Stretchable Silver Nanowire Conductors. *Adv. Mater.* **2012**, 24, 5117–5122.